Nanoscale Horizons

ROYAL SOCIETY OF CHEMISTRY

COMMUNICATION

View Article Online
View Journal | View Issue

Cite this: *Nanoscale Horiz.*, 2022, 7, 908

Received 19th May 2022,
Accepted 7th June 2022

DOI: 10.1039/d2nh00243d

rsc.li/nanoscale-horizons

Multicomponent encapsulation into fully degradable protein nanocarriers *via* interfacial azide–alkyne click reaction in miniemulsion allows the co-delivery of immunotherapeutics†

Natkritta Hüppe,[a] Jenny Schunke,[b] Michael Fichter,[ab] Volker Mailänder,[ab] Frederik R. Wurm *[ac] and Katharina Landfester *[a]

Encapsulation of multiple adjuvants along with antigens into nanocarriers allows a co-delivery to antigen-presenting cells for the synergistic induction of robust immune responses. However, loading cargoes of different molar masses, polarities, and solubilities in high efficiencies remains a challenge. Therefore, we developed a strategy to encapsulate a triple combination of the so-called adjuvants, *i.e.* with Resiquimod (R848), muramyl dipeptide (MDP) and polyinosinic-polycytidylic acid (Poly(I : C)) into human serum albumin (HSA) nanocarriers. The loading is conducted *in situ* while the nanocarrier is formed by an orthogonal and metal-free click reaction at the interface of an inverse miniemulsion. By this unique approach, high encapsulation efficiency without harming the cargo during the nanocarrier formation process and regardless of their physical properties is achieved, thus keeping their bioactivity. Furthermore, we demonstrated high control over the encapsulation efficiency and varying the amount of each cargo did not influence the efficiency of multicomponent encapsulation. Azide-modified HSA was crosslinked with hexanediol dipropiolate (HDDP) at the interface of a water-in-oil miniemulsion. Varying the crosslinker amount allowed us to tailor the density and degradation rates of the protein shell. Additional installation of disulfide bonds into the crosslinker created redox-responsive nanocarriers, which degraded both by protease and under reducing conditions with dithiothreitol. The prepared HSA nanocarriers were efficiently taken up by dendritic cells and exhibited an additive cell activation and maturation, exceeding the nanocarriers loaded with only a single drug. This general protocol allows the orthogonal and metal-free encapsulation of various drugs or adjuvants at defined concentrations into the protein nanocarriers.

New concepts

In this work, we demonstrated an efficient *in situ* encapsulation of up to four cargo molecules with different molar mass and solubility into protein nanocarriers, allowing co-delivery of multiple therapeutics for a synergistic therapeutic effect. The novel combination of a reductive-responsive crosslinker with enzymatically degradable proteins as the nanocarrier material created a dual-responsive nanocarrier with complete degradability and release rates in cells. A metal-free azide-alkyne crosslinking chemistry for the formation of the protein nanocarriers ensures a mild and biorthogonal encapsulation of sensible cargoes where their bioactivity is preserved. The developed inverse miniemulsion process enables multicomponent encapsulation of a broad range of cargoes from small to large, hydrophilic to hydrophobic and inorganic, in numerous possible combinations to achieve multifunctional nanocarriers for a broad range of applications, from biomedicine to material science.

Introduction

Biochemical processes in the body rely on a complex interplay of multiple components. If medical therapy aims to mimic or enhance those processes, multiple therapeutic components have to be integrated into one system. For example, in immunotherapy, the biggest challenge is the exhaustion of immune cells due to the immunosuppressive tumor microenvironment.[1–3] Hence, effective tumor treatment relies on the induction of a strong and durable immune response. Monotherapy proved to be insufficient to overcome these challenges and efforts have to be made to realize a combinatorial treatment with multiple components.[4,5] True to the motto "The more the merrier", a combination of multiple

[a] *Max Planck Institute for Polymer Research, Ackermannweg 10, 55128 Mainz, Germany. E-mail: landfester@mpip-mainz.mpg.de*
[b] *Department of Dermatology, University Medical Center Mainz, Langenbeckstraße 1, 55131 Mainz, Germany*
[c] *Sustainable Polymer Chemistry, Department of Molecules and Materials, Faculty of Science and Technology, MESA + Institute for Nanotechnology, University of Twente, Drienerlolaan 5, 7522 NB Enschede, The Netherlands. E-mail: frederik.wurm@utwente.nl*

† Electronic supplementary information (ESI) available. See DOI: https://doi.org/10.1039/d2nh00243d

components enables additive effects for enhanced treatment efficacy. In vaccination approaches, a combination of multiple adjuvants yields a synergistic effect in dendritic cell-directed T cell stimulation, increasing the vaccination effect.[6–9]

The key to success is an efficient process for multicomponent encapsulation of cargoes with different physicochemical properties such as molar mass, polarity, and solubility.

Common methods to prepare protein nanocarriers include desolvation, self-assembly or gelation. For example, Abraxane® is a nanoparticle based on albumin-bound paclitaxel, which is commercially used in cancer therapy. Paclitaxel is entrapped into the albumin nanoparticle during the albumin aggregation by a desolvation process. Although efficient entrapment of drugs can be achieved with those methods, there is a lack of control when multiple drugs should be encapsulated simultaneously into one nanocarrier. Especially when the cargo molecules have different physicochemical properties such as solubility, controlled and efficient encapsulation of all components is challenging with methods relying on random entrapment.

To design the optimal nanocarrier, several requirements are necessary: (1) simultaneous encapsulation of multiple cargoes, (2) selective reaction for the shell formation without harming the cargo, (3) dense carriers for the transport in the body, and (4) degradation of the carriers at the target site. Combining all requirements in one process proved to be challenging. Our developed process combines all four requirements and enables controlled and efficient multicomponent encapsulation into fully degradable protein nanocarriers (PNCs) *via* azide–alkyne click reaction in inverse miniemulsion (Fig. 1).

For the first requirement, an inverse miniemulsion allows the simultaneous encapsulation of different water-soluble cargo molecules into nanocarriers with a defined concentration.[10] In an inverse miniemulsion, the shell material is crosslinked at the interface of the water-droplets *via* an oil-soluble crosslinker, forming a nanocarrier with a liquid core. The water-soluble cargo molecules are encapsulated inside the nanocarriers during the interfacial shell formation. For the second requirement, click reactions enable selective linkage between shell material and crosslinker without involving the cargo in the shell formation reaction.[11,12] Previously, protein nanocarriers were prepared by UV-initiated photoclick tetrazole-ene reaction in inverse miniemulsion.[13] However, UV-light or other harsh initiators, such as metals,[14] can destroy sensitive cargoes leading to loss of bioactivity. A crosslinker such as hexanediol dipropiolate (HDDP) with an activated alkyne reacts without a catalyst in an azide–alkyne click reaction.[15,16] The amount of crosslinker influences the number of links between the shell material and might control the density of the nanocarrier shell for the third requirement. The last requirement is a degradable shell material ensuring the release of the cargo from nanocarriers. Proteins have been widely used as nanocarrier materials, because of their natural biocompatibility and degradability.[13,17–19]

Results and discussion

For the azide–alkyne click reaction, human serum albumin (HSA) was functionalized at the lysine residue by a metal-free transfer reaction into azide groups using 1-imidazol azide hydrochloride.[20] After functionalization, the fluorescamine assay showed that about 19–24 amines of the 59 lysine residues per HSA (30–35 accessible lysines) were transformed into azides. The degree of functionalization changed with pH value as lower pH values led to lower nucleophilicity of the amine and less transfer reactions, whereas pH 9.5 gave an optimal balance between yielding high number of transfers and maintaining the protein structure (Table S1, ESI†). A comparison of the IR

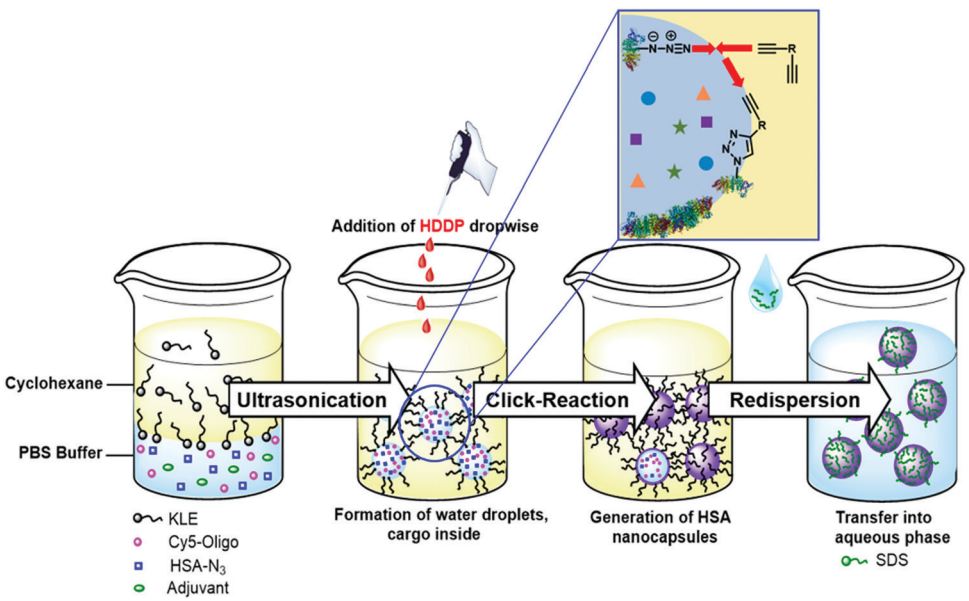

Fig. 1 Multicomponent encapsulation into protein nanocarriers through interfacial azide–alkyne crosslinking in inverse miniemulsion.

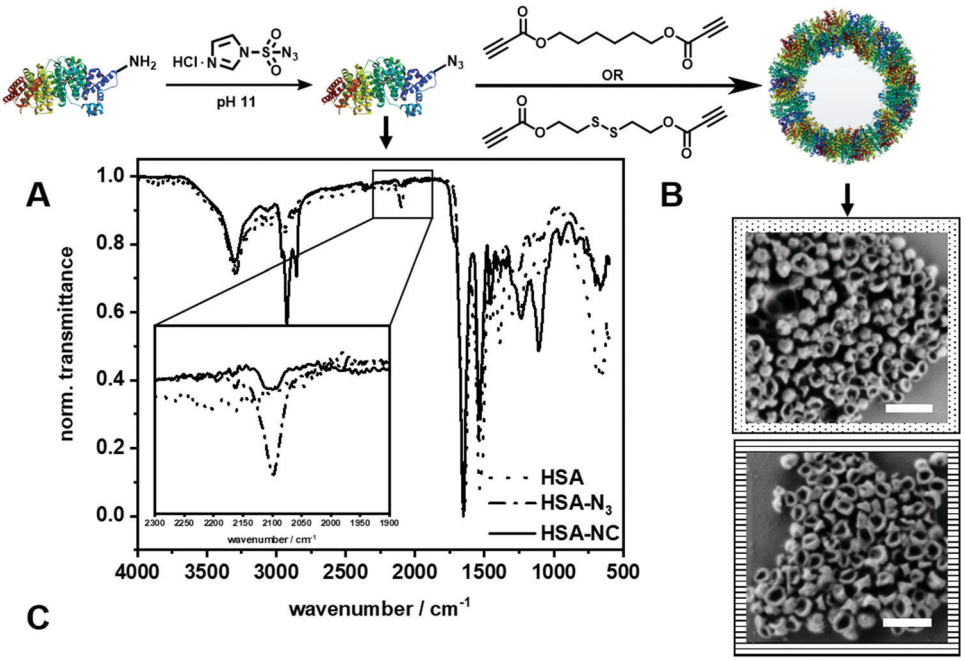

Protein	N_{theo} (NH_2)	N_{ex} (NH_2)	N_{ex} (N_3)	Linker	$d_{i,CH}$ / nm	PDI_{CH}	$d_{i,water}$ / nm	PDI_{water}	ζ /mV
HSA	30-35	11	19-24	HDDP	302	0.13	264	0.23	-30 ±2
HSA	30-35	11	19-24	HDDP-SS	327	0.14	254	0.17	-34±2

Fig. 2 Reaction scheme for the formation of protein nanocarriers through azide–alkyne click reaction (top). (A) IR spectra of native (···), azide-functionalized (-·-) and human serum albumin nanocarriers (—). (B) SEM images of HSA-NCs using a HDDP (□) and HDDP-SS (□) ratio (Scale bar: 0.5 μm). (C) Analytic data of HSA NCs using HDDP and HDDP-SS.

spectra of natural and azide-modified HSA showed successful modification as demonstrated by the presence of the characteristic azide signal at 2100 cm^{-1} (Fig. 2A). Furthermore, no significant changes in the secondary structure of the protein were observed by CD spectroscopy (Fig. S6, ESI†). Therefore, the modified protein remained highly water-soluble (>100 mg mL^{-1}) further highlighting the mild conditions during the transfer reaction. When the "azidation" was conducted with the horseradish peroxidase (HRP) Table S2 and Fig. S17, ESI† the enzymatic activity was reduced by 40%, probably due to the high basic pH of 11 during the transfer reaction (Fig. S19, ESI†).

For the formation of protein nanocarriers by azide–alkyne click reaction, we chose the dialkyne hexanediol dipropiolate (HDDP) as a crosslinker of the azide-modified proteins. The carbonyl group located next to the alkyne moiety activates the alkyne by an inductive effect, allowing a click reaction without using a metal catalyst.[15] Moreover, inserting a disulfide bond into the chemical structure of HDDP (*i.e.* to HDDP-SS, *cf.* Fig. 2) created a crosslinker prone to degradation by a reducing agent.[16]

The PNCs were prepared in an inverse water-in-oil miniemulsion with cyclohexane as the continuous and an aqueous buffer as the dispersed phase (Scheme S2, ESI†). The aqueous nanodroplets were prepared with high shear forces using ultrasonication and were stabilized by the surfactant P((E/B)-*b*-EO) (KLE).[21] The protein shell formed through an interfacial crosslinking by click reaction at the water droplet interface after addition of HDDP or HDDP-SS to the inverse miniemulsion. In the IR spectra of the PNCs, the azide signal at 2100 cm^{-1} decreased due to the formation of the triazol during the click reaction (Fig. 2A). The hydrodynamic diameters of the PNCs (d_h) in cyclohexane were determined to be approx. 300 nm by dynamic light scattering (DLS). After redispersion in water using sodium dodecyl sulfate (SDS, 0.02 mM) as the surfactant followed by washing, the diameters decreased to approx. 250 nm with a zeta potential of approx. −30 mV (Fig. 2C and Table S4, ESI†). Scanning electron micrographs and transmission electron micrographs revealed a core-shell morphology of the PNCs (Fig. 2B and Fig. S8, ESI†). In addition, the PNCs based on HRP exhibited similar results in size and morphology (Fig. S17 and S18, ESI†). This demonstrated the excellent reproducibility and transferability for forming PNCs by the developed protocol. Moreover, the HRP nanocarriers were still enzymatically active, showing approx. 60% of the native enzyme activity (Fig. S19, ESI†).

By varying the amount of HDDP crosslinker, shell thickness and size of PNCs could be controlled (Fig. 3). When the

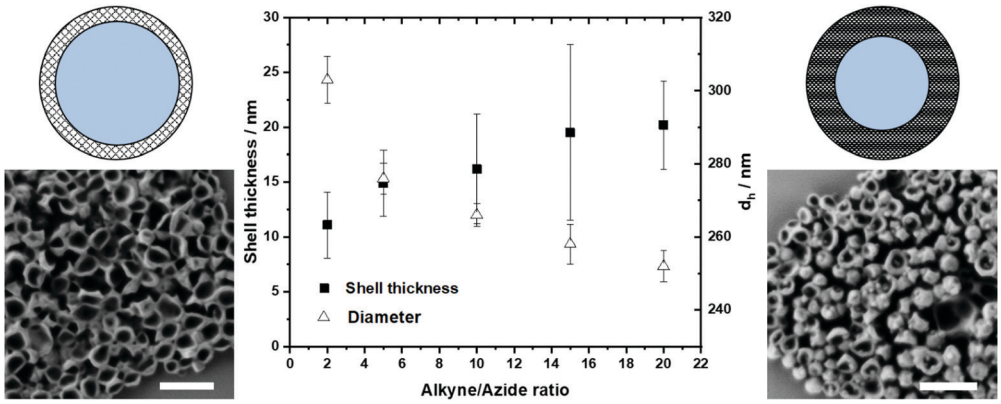

Fig. 3 Influence of alkyne : azide ratio on the shell thickness (■) and diameter (Δ) of protein nanocarriers. Scanning electron micrographs of HSA nanocarriers using a 2 : 1 (left) and 20 : 1 (right) ratio (Scale bar: 0.5μm).

interfacial crosslinking of azide-modified protein with HDDP was performed with an alkyne : azide ratio of 20 : 1, PNCs with a d_h = 250 nm and approx. 20 nm shell thickness were obtained. With a lower alkyne: azide ratio, the shell thickness decreased, while the diameters increased, probably due to an increased swelling of the softer protein shell (Fig. 3). The amount of crosslinker used additionally influenced the encapsulation efficiency after water transfer. The encapsulation efficiency of dextran-sulforhodamine B (M = 10 kDa) decreased from 62% to 39% when 20 equiv. HDDP or only 2 equiv. HDDP were used, respectively, to prepare the PNCs. By encapsulating the low molecular weight dye sulfurhodamine-101 (M = 606.71 g mol^{-1}), a lower crosslinking density was detected, leading to a faster diffusion through the nanocarrier shell, probably attributed to the thinner and looser shell walls when low amounts of HDDP were used (Fig. S12, ESI†).

The degradation of the PNCs was investigated by monitoring the release of dextran-rhodamine B (M = 10 kDa, λ_{em} = 570 nm) under different conditions. Crosslinking with different amounts of HDDP or HDDP-SS enabled investigating the influence of shell density on the degradation kinetics. The HSA-NCs degraded upon the addition of proteinase K (5 U mL^{-1}) and the amount of released dye was detected in the aqueous supernatant. Depending on the time of the degradation experiment, the amount of released dye increased and reached a plateau of approx. 90% dye after 96 h in all cases (Fig. 4A). However, the crosslinking density, *i.e.* the amount of HDDP used during the PNC formation, influenced the degradation rate of the protein shell and thus the release of the dye. Time and crosslinker dependence of dye-release was also observed for the enzymatic degradation of PNCs crosslinked with HDDP-SS (Fig. 4B). The HSA-HDDP-SS NCs could be cleaved by proteinase K as well as under reducing conditions, *e.g.* by adding dithiothreitol (DTT) as a reducing agent. The PNCs crosslinked with different amounts of HDDP-SS were treated with proteinase K (2 U mL^{-1}) and DTT (3 mM), respectively and in combination, and the amount of released dextran-rhodamine B was measured over time, indicating the

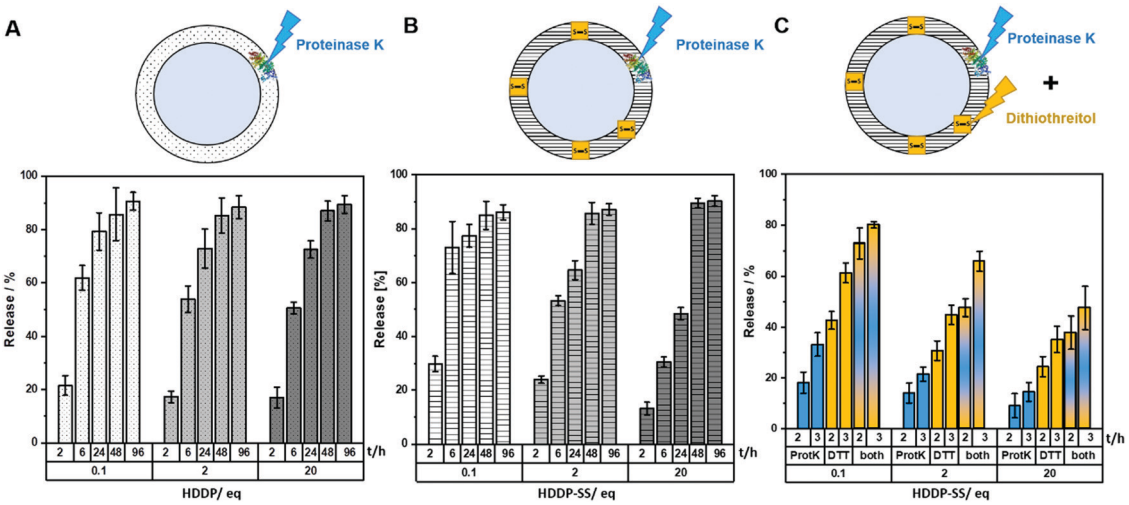

Fig. 4 Release kinetics of dextran-rhodamine B (10 kDa) from HSA NCs prepared with different crosslinking densities as indicated by the ratio of HDDP or HDDP-SS/equiv.: (A) PNCs crosslinked with HDDP and degraded with proteinase K (5 U mL^{-1}), (B) PNCs crosslinked with HDDP-SS and degraded with proteinase K (5 U mL^{-1}), (C) PNCs crosslinked with HDDP-SS and degraded with proteinase K (blue, 5 U mL^{-1}) and dithiothreitol (yellow, 3 mM).

release kinetics were influenced by the crosslinking degree. The resulting PNCs crosslinked with HDDP-SS obtained the property of dual-degradation by DTT and proteinase K.

The degradation of the PNCs was also visible by the naked eye, as the turbid PNCs dispersion completely cleared up upon DTT addition (Fig. S15, ESI†). DLS was applied to further quantify the degradation rates of PNCs: Following treatment with proteinase K and DTT, respectively, the size of the NCs decreased significantly from 254 nm to 71 nm with a broadening of the polydispersity index to >0.4 (Fig. S13 and S14, ESI†). Additionally, the derived count rate (DCR) decreased significantly during the degradation experiment, indicating the formation of smaller fragments with lower scattering intensity. The derived count rate was monitored upon DTT treatment and continuously decreased to the lower limit of the DLS apparatus indicating an almost complete degradation of the PNCs (Fig. S15, ESI†).

Since anti-tumor vaccination still lacks the effective response of immune cells against tumors in most cases of vaccinated patients, the role of nanocarriers for co-delivery of vaccine components needs to step into focus. In the vaccination process, the vaccine, consisting of antigen and adjuvants, is taken up by dendritic cells and the antigens are presented on major histocompatibility complex (MHC) molecules of the DCs to the T cells.[22,23] Subsequently, antigen-specific T cells are activated and proliferate to attack cells bearing the tumor-specific antigen eventually leading to tumor cell killing.[24] Crucial for the success of T cell priming is a strong activation of antigen-presenting cells (*e.g.* DCs) by adjuvants inducing expression of costimulatory molecules and the release of activating pro-inflammatory cytokines. Choosing the correct type and application route of adjuvants is of great importance for the induction of robust immune responses as each adjuvant bind to distinct receptors triggering different signaling pathways in antigen-presenting cells.[25,26] Therefore, a combination of several different adjuvants simultaneously stimulates different receptors, leading to an additive DC activation.[27] To achieve a high local concentration of adjuvants in one DC, all components must be delivered simultaneously.[18]

Resiquimod (R848) is a small molecule (M = 350.8 g mol^{-1}) with low water-solubility (>1 mg mL^{-1}) and acts as an agonist for the toll-like receptors (TLR) 7 and 8.[28] The water-soluble peptidoglycan muramyl dipeptide (MDP; M = 492.5 g mol^{-1}) has been shown to be recognized by nucleotide-binding oligomerization domain-containing protein (NOD) 2.[29] The double-stranded RNA mimic polyinosinic : cytodylic acid (Poly(I : C); 0.2–1 kb) acts as a TLR 3 ligand.[30] A major challenge is to find a compatible protocol for the multicomponent encapsulation of cargoes with such different properties in terms of solubility and molecular weight. In this study, we combined R848, MDP, and Poly(I : C) and added Cy5-Oligo (5 kDa) as an additional cargo acting as a fluorescent dye (Fig. 5A), allowing us to investigate the cellular uptake of PNCs by DCs. All four components were successfully encapsulated into PNCs through the azide–alkyne click reaction in inverse miniemulsion demonstrating the excellent feasibility of developed nanocarrier formation for the encapsulation of multiple components. Even though dimethyl sulfoxide (DMSO) was used as a solvent for R848 (14 vol% in the disperse phase) stable droplets could be formed with no influence on the interfacial protein shell

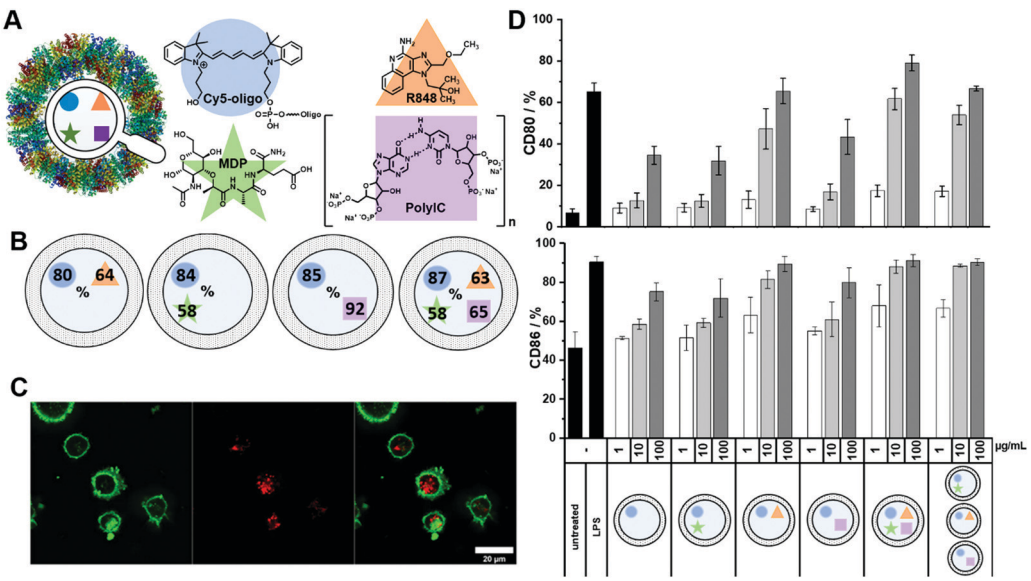

Fig. 5 (A) Chemical structures of Cy5-Oligo dye (●) and adjuvants R848 (▲), MDP (★) and Poly(I : C) (■) encapsulated into HSA NCs. (B) Encapsulation efficiency of cargoes in different combinations into HSA NCs crosslinked with HDDP in percent. (C) Confocal laser scanning microscopy images of bonemarrow-derived dendritic cells (green) and ingested HSA NCs (red). (D) Upregulation of DC maturation markers CD80 and CD86 after stimulation with adjuvant-loaded HSA NCs with either single loading, triple loading or a mixture of single-loaded NCs. BMDCs (2 × 10^5 cells per mL) were incubated with differently loaded HSA NC formulations (1–100 µg mL^{-1}) or lipopolysaccharid (LPS) (100 ng mL^{-1}) as a positive control for 24 h. Surface expression of CD80 and CD86 of PNC-treated BMDCs was measured by flow cytometry.

formation. With such different cargoes, each one needed a specific quantification assay to calculate their EE into the PNCs. The UV-active cargoes, Cy5-Oligo and R848, were quantified through UV/Vis measurements using a standard calibration (Fig. S10 and S20, ESI†). Due to the *N*-acetylglucosamide moiety present within the MDP, a quantification by a modified Morgan–Elson Reaction assay, which was devised for this study, was performed (Fig. S21, ESI†). HPLC was used for the quantification of Poly(I:C) (Fig. S22, ESI†). The PNCs were degraded by proteinase K (30 U mL^{-1}, 24 h, 37 °C), filtered, and the amount of each cargo was measured in the supernatant. Comparable EEs were obtained for the small molecules R848, and MDP (up to 65%) and Cy5-Oligo (over 80%) independent from cargo-loading (Fig. 5B). Only the EE of the high molecular weight Poly(I:C) decreased significantly from approx. 90% for single-loaded PNCs to approx. 60% for multiple-loaded PNCs. Table S4 (ESI†) summarizes the encapsulation efficiencies and the characterization data for all HSA NCs prepared herein: In all cases, similar zeta potentials between −30 and −40 mV were determined, indicating a similar shell formation regardless of the cargo molecule or its charge, *i.e.* an efficient encapsulation inside of the NCs was achieved. The diameters for all "clicked" NCs were similar and detected between 200–300 nm (after redispersion in water, measured by DLS). To show control over the simultaneous encapsulation of multiple cargo molecules into the crosslinked protein nanocapsules, we varied the amount of each adjuvant and ratios between payloads and quantified the encapsulation efficiency (Table S4, ESI†). For MDP and Poly(I:C) no significant difference in encapsulation efficiency could be observed when varying their amount, independent if MDP and Poly(I:C) were encapsulated alone or in the triple combination. Only in one case, the encapsulation efficiency of the different cargo molecules were affected. When a high amount of R848 was used, the encapsulation efficiency of all payloads decreased significantly. This could be a result of higher concentration of DMSO in the dispersed phase, which influences the solubility of the payloads in the droplet and thus the encapsulation efficiency. Nevertheless, if the amount of DMSO is kept to a minimum, our developed approach demonstrated high control over the encapsulation efficiency of the multiple payloads and thus control over the concentration and ratios of payload inside the capsules.

Flow cytometric and confocal laser scanning analyses revealed an efficient uptake of the adjuvant-loaded PNCs by the bone marrow-derived dendritic cells (BMDC) *in vitro*, as detected through the fluorescence of Cy5-Oligo (Fig. 5C and Fig. S22, ESI†). The co-delivery of the adjuvant combination by PNCs was evaluated by the amount of cell surface-expressed activation markers CD80 and CD86 on the BMDCs after incubation with PNCs for 24 h (Fig. 5C). Untreated cells served as a negative control whereas cells treated with lipopolysaccharide (LPS), a potent TLR4 agonist inducing high expression of DC maturation, served as a positive control. The expression of CD80 and CD86 increased after treatment with adjuvant-loaded PNCs compared to untreated cells or cells treated with empty PNCs. Among the single-loaded PNCs with either R848, MDP or Poly(I:C), the TLR7/8 ligand R848 yielded the highest stimulation of BMDCs. The expression of the surface markers increased with PNCs loaded with the triple-combination of adjuvants compared to single-loaded PNCs. Moreover, a mixture of single-loaded PNCs with R848, MDP and Poly(I:C), respectively, exhibited a lower expression of surface markers compared to equimolar amounts of all three adjuvants encapsulated into one PNCs demonstrating a higher stimulation through co-delivery.

The *in vitro* results underline the importance of simultaneous delivery of cargoes by multicomponent encapsulation into nanocarrier to achieve higher effectivity in nanocarrier-based vaccination approaches. With our developed protein nanocarrier combining all the nanocarrier design requirements, we could encapsulate and co-deliver multiple components independent of molecular weight (low-high), solubility, or material (also inorganic).

Conclusion

We developed a bioorthogonal protocol for the multicomponent encapsulation and co-delivery of fully-biodegradable protein nanocarriers. For the synthesis of the PNCs, we applied a metal-free protocol to modify the protein's amine groups to azide groups with 1-sulfurylimidazol hydrochloride in water. With an azide-modified protein on hand, human serum albumin nanocarriers were prepared by metal-free azide–alkyne click reaction with activated hexanediol dipropiolate in an inverse miniemulsion. The developed process enabled the simultaneous encapsulation of multiple cargoes with different physicochemical properties such as molecular weights and solubility. A high encapsulation efficiency and a preserved bioactivity of the cargo was obtained. Comparable encapsulation efficiency of each adjuvant was achieved, independent of the amount and ratios of the cargo molecules. Varying the crosslinker amount not only allowed to tailor the density of the shell to entrap different adjuvants, but also the degradation and release rates of the nanocarriers. PNCs were further equipped with disulfide bonds by using HDDP-SS as the crosslinker, which resulted in nanocarriers releasing the cargo enzymatically and under reductive conditions. We demonstrated a successful encapsulation of the adjuvants R848, MDP, and Poly(I:C) into PNCs yielding a higher stimulation of immune cells with co-delivery of all three adjuvants encapsulated into one nanocarrier compared to single-loaded PNCs. In summary, this protocol might be used to develop efficient immunotherapies, which rely on the combination of several drugs and adjuvants with highly different phöysical properties. Further, the bioorthogonal formation of the nanocarriers with a guaranteed release upon proteolysis might be a powerful tool for the delivery of nucleic acids.

Conflicts of interest

There are no conflicts to declare.

Acknowledgements

This work was funded by the DFG/SFB1066 ('Nanodimensional polymer therapeutics for tumor therapy'). We thank Gunnar Glasser (MPIP) and Christoph Sieber (MPIP) for electron microscopy, Stephan Türk (MPIP) for mass spectrometry, Michael Steiert (MPIP) for ICP-OES and Beate Müller (MPIP) for HPLC measurements. We want to acknowledge Katja Klein (MPIP) and Sabrina Brand (MPIP) for support in synthesis and Marina Machtakova (MPIP) for enzyme activity tests. Open Access funding provided by the Max Planck Society.

References

1 M. E. Pichichero, Challenges in vaccination of neonates, infants and young children, *Vaccine*, 2014, **32**(31), 3886–3894.
2 R. Aspinall, G. Del Giudice, R. B. Effros, B. Grubeck-Loebenstein and S. Sambhara, Challenges for vaccination in the elderly, *Immun. Ageing*, 2007, **4**(1), 1–9.
3 S. H. van der Burg, R. Arens, F. Ossendorp, T. van Hall and C. J. Melief, Vaccines for established cancer: overcoming the challenges posed by immune evasion, *Nat. Rev. Cancer*, 2016, **16**(4), 219–233.
4 S. Valastyan and R. A. Weinberg, Tumor metastasis: molecular insights and evolving paradigms, *Cell*, 2011, **147**(2), 275–292.
5 O. Veiseh, F. M. Kievit, R. G. Ellenbogen and M. Zhang, Cancer cell invasion: treatment and monitoring opportunities in nanomedicine, *Adv. Drug Delivery Rev.*, 2011, **63**(8), 582–596.
6 T. Warger, P. Osterloh, G. Rechtsteiner, M. Fassbender, V. Heib, B. Schmid, E. Schmitt, H. Schild and M. P. Radsak, Synergistic activation of dendritic cells by combined Toll-like receptor ligation induces superior CTL responses *in vivo*, *Blood*, 2006, **108**(2), 544–550.
7 M. Roelofs, L. Joosten, S. Abdollahi-Roodsaz, A. Van Lieshout, T. Sprong, F. Van Den Hoogen, W. Van Den Berg and T. Radstake, The expression of toll-like receptors 3 and 7 in rheumatoid arthritis synovium is increased and costimulation of toll-like receptors 3, 4, and 7/8 results in synergistic cytokine production by dendritic cells, *Arthritis Rheum.*, 2005, **52**(8), 2313–2322.
8 A. I. Tukhvatulin, A. S. Dzharullaeva, N. M. Tukhvatulina, D. V. Shcheblyakov, M. M. Shmarov, I. V. Dolzhikova, P. Stanhope-Baker, B. S. Naroditsky, A. V. Gudkov and D. Y. Logunov, Powerful complex immunoadjuvant based on synergistic effect of combined TLR4 and NOD2 activation significantly enhances magnitude of humoral and cellular adaptive immune responses, *PLoS One*, 2016, **11**(5), e0155650.
9 C. Da Silva, M. Camps, T. Li, A. Chan, F. Ossendorp and L. Cruz, Co-delivery of immunomodulators in biodegradable nanoparticles improves therapeutic efficacy of cancer vaccines, *Biomaterials*, 2019, **220**, 119417.
10 K. Landfester and C. K. Weiss, Encapsulation by Miniemulsion Polymerization, *Modern Techniques for Nano- and Microreactors/-reactions*, 2010, pp. 1–49.
11 H. C. Kolb, M. Finn and K. B. Sharpless, Click chemistry: diverse chemical function from a few good reactions, *Angew. Chem., Int. Ed.*, 2001, **40**(11), 2004–2021.
12 J. E. Moses and A. D. Moorhouse, The growing applications of click chemistry, *Chem. Soc. Rev.*, 2007, **36**(8), 1249–1262.
13 K. Piradashvili, J. Simon, D. Paßlick, J. R. Höhner, V. Mailänder, F. R. Wurm and K. Landfester, Fully degradable protein nanocarriers by orthogonal photoclick tetrazole–ene chemistry for the encapsulation and release, *Nanoscale Horiz.*, 2017, **2**(5), 297–302.
14 L. M. Gaetke and C. K. Chow, Copper toxicity, oxidative stress, and antioxidant nutrients, *Toxicology*, 2003, **189**(1-2), 147–163.
15 J. M. Siebert, G. Baier, A. Musyanovych and K. Landfester, Towards copper-free nanocapsules obtained by orthogonal interfacial ''click'' polymerization in miniemulsion, *Chem. Commun.*, 2012, **48**(44), 5470–5472.
16 G. Baier, M. Fichter, A. Kreyes, K. Klein, V. Mailander, S. Gehring and K. Landfester, Glutathione Responsive Hyaluronic Acid Nanocapsules Obtained by Bioorthogonal Interfacial ''Click'' Reaction, *Biomacromolecules*, 2016, **17**(1), 148–153.
17 M. Tarhini, H. Greige-Gerges and A. Elaissari, Protein-based nanoparticles: From preparation to encapsulation of active molecules, *Int. J. Pharm.*, 2017, **522**(1-2), 172–197.
18 D. Paßlick, K. Piradashvili, D. Bamberger, M. Li, S. Jiang, D. Strand, P. R. Wich, K. Landfester, M. Bros and S. Grabbe, Delivering all in one: Antigen-nanocapsule loaded with dual adjuvant yields superadditive effects by DC-directed T cell stimulation, *J. Controlled Release*, 2018, **289**, 23–34.
19 M. Neek, T. I. Kim and S.-W. Wang, Protein-based nanoparticles in cancer vaccine development, *Nanomedicine*, 2019, **15**(1), 164–174.
20 E. D. Goddard-Borger and R. V. Stick, An efficient, inexpensive, and shelf-stable diazotransfer reagent: imidazole-1-sulfonyl azide hydrochloride, *Org. Lett.*, 2007, **9**(19), 3797–3800.
21 A. Thomas, H. Schlaad, B. Smarsly and M. Antonietti, Replication of lyotropic block copolymer mesophases into porous silica by nanocasting: Learning about finer details of polymer self-assembly, *Langmuir*, 2003, **19**(10), 4455–4459.
22 A. Gardner and B. Ruffell, Dendritic cells and cancer immunity, *Trends Immunol.*, 2016, **37**(12), 855–865.
23 K. Ni and H. O'neill, The role of dendritic cells in T cell activation, *Immunol. Cell Biol.*, 1997, **75**(3), 223–230.
24 J. Couzin-Frankel, Cancer immunotherapy, *Am. Assoc. Adv. Sci.*, 2013, **342**, 1432–1433.
25 E. S. Bergmann-Leitner and W. W. Leitner, Adjuvants in the driver's seat: how magnitude, type, fine specificity and longevity of immune responses are driven by distinct classes of immune potentiators, *Vaccines*, 2014, **2**(2), 252–296.
26 S. G. Reed, M. T. Orr and C. B. Fox, Key roles of adjuvants in modern vaccines, *Nat. Med.*, 2013, **19**(12), 1597–1608.
27 B. Guy, The perfect mix: recent progress in adjuvant research, *Nat. Rev. Microbiol.*, 2007, **5**(7), 396–397.

28 M. Jurk, F. Heil, J. Vollmer, C. Schetter, A. M. Krieg, H. Wagner, G. Lipford and S. Bauer, Human TLR7 or TLR8 independently confer responsiveness to the antiviral compound R-848, *Nat. Immunol.*, 2002, **3**(6), 499.
29 S. E. Girardin, I. G. Boneca, J. Viala, M. Chamaillard, A. Labigne, G. Thomas, D. J. Philpott and P. J. Sansonetti, Nod2 is a general sensor of peptidoglycan through muramyl dipeptide (MDP) detection, *J. Biol. Chem.*, 2003, **278**(11), 8869–8872.
30 L. Alexopoulou, A. C. Holt, R. Medzhitov and R. A. Flavell, Recognition of double-stranded RNA and activation of NF-κB by Toll-like receptor 3, *Nature*, 2001, **413**(6857), 732–738.